COMMUNICATION

Organic Single Crystal Field-effect Transistors Based on 6*H*-pyrrolo[3,2–*b*:4,5–*b́*]bis[1,4]benzothiazine and its Derivatives

By *Zhongming Wei, Wei Hong, Hua Geng, Chengliang Wang, Yaling Liu, Rongjin Li, Wei Xu,* Zhigang Shuai,* Wenping Hu,* Quanrui Wang,* and *Daoben Zhu**

With the advantages of flexibility and large-area fabrication, organic semiconductors have shown tremendous potential for future applications in organic optoelectronics. One of the most representative and extensive applications within this field developed over the past decades have been organic field-effect transistors (OFETs).[1,2] The development of OFETs has focused on the design and synthesis of novel materials, the fabrication of high performance devices, and the understanding of device physics, and principles of charge transport.[3–6] Among these works, single-crystal field-effect transistors (SCFETs) have attracted considerable attention as they offer insight into the intrinsic charge transport properties in organic semiconductors, which have already become a strong tool for exploring the structure–property relationships.[7–22] Recently, we reported the thin film transistors based on a pentacene analogue: 6*H*-pyrrolo-[3,2–*b*:4,5–*b́*]bis[1,4]benzothiazine and its 6-substituted derivatives (PBBTZ **1–3**, see Scheme 1).[23] A high mobility up to $0.35\,cm^2\,V^{-1}\,s^{-1}$ and an on/off ratio of around 1.5×10^7 have been obtained from the devices of **1**. Moreover, these materials also display other advantages such as facile synthesis and increased stability compared with that of pentacene. All these imply the promising potential of the PBBTZ series in organic electronics. Hence, it is worth to further explore these materials to reveal their structure–property relationships by SCFET studies through detailed investigations on the single-crystal structures and quantum chemical calculations of the main parameters related to the charge transport.

[*] Z. Wei, H. Geng, C. Wang, Dr. Y. Liu, Dr. R. Li, Dr. W. Xu, Prof. Z. Shuai, Prof. W. Hu, Prof. D. Zhu
Beijing National Laboratory for Molecular Sciences
Key Laboratory of Organic Solids, Institute of Chemistry
Chinese Academy of Sciences
Beijing 100190 (P. R. China)
E-mail: wxu@iccas.ac.cn; zgshuai@iccas.ac.cn; huwp@iccas.ac.cn
Z. Wei, C. Wang
Graduate University of the Chinese Academy of Sciences
Beijing 100039 (P. R. China)
Dr. W. Hong, Prof. Q. Wang
Department of Chemistry, Fudan University
Shanghai 200433 (P. R. China)

DOI: 10.1002/adma.201000088

Here, we report SCFETs based on single crystalline sub-micrometer sized ribbons of PBBTZ **1–3**. All the SCFETs show higher mobilities than their corresponding thin film transistors of the same materials. Excellent performance with a mobility as high as $3.6\,cm^2\,V^{-1}\,s^{-1}$ and an on/off ratio larger than 10^6 was obtained from the device of **1**. Moreover, excellent environmental stability was also observed for the SCFETs of **1**. The substitution on the central pyrrole *N*-atom had a large influence both on the crystal structure and the SCFET performance, which are experimentally and theoretically discussed.

Single-crystalline sub-micrometer ribbons of **1–3** were grown by physical vapor transport processes.[24] As shown in Figures 1a, d, and g, the single crystalline ribbons have a width from hundreds of nanometers to several micrometers, and a length from tens to hundreds of micrometers. The individual single-crystalline ribbons were further investigated by transmission electron microscopy (TEM) (Fig. 1b, e, and h) and selected-area electron diffraction (SAED) (Fig. 1c, f, and i) to define the growing habits. The measured spaces from the SAED patterns were in good agreement with the crystallographic data of large-scale single crystals. The diffraction spots suggest that the growth direction of the **1** single-crystalline ribbon was [100] (i.e., *a* axis), as shown in Figure 1c. When substituted with phenyl and alkyl groups, the growth directions of single-crystalline ribbons of **2** and **3** were changed to [010] (i.e., *b* axis), as shown in Figures 1f and i. The electron diffraction data agreed well with the morphologies theoretically predicted by the Bravais–Friedel–Donnay–Harker (BFDH) method as shown in the left of Figure S3 (see Supporting Information). For these three crystals, the primary growth directions were all along the π-stacking directions as shown to the right of Figure S3. This indicates that the strong π–π interactions between the adjacent molecules may play a dominant role in the growth of the **1–3** single crystalline ribbons. It has been addressed that organic thin films or crystals with the intermolecular π-stacking directions parallel to the conducting channel of the OFETs would result in a high performance because of the efficient overlap of the intermolecular π-orbits.[1] For details of the intermolecular π–π interactions and molecular overlaps in the single crystals of **1–3**, see the Supporting Information.

The SCFETs based on **1–3** single crystalline ribbons grown on octadecyltrichlorosilane (OTS)-treated Si/SiO_2 substrates were fabricated. Thin Au films (~100 nm thick) were glued in situ onto the individual ribbons[10,25] and functioned as source/drain

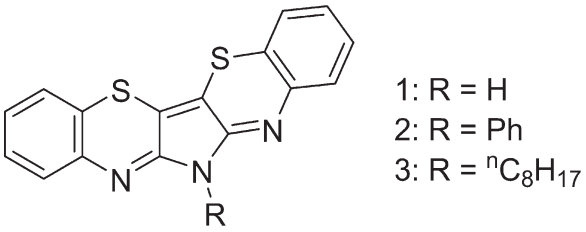

Scheme 1. Molecular structures of PBBTZ **1–3**.

electrodes. Figure 2a shows the schematic structure of a SCFET device fabricated by such a method. Figure 2b–d show the corresponding scanning electron microscopy (SEM) images of the SCFET devices. All the SCFETs showed p-type properties under ambient conditions. Typical transfer and output characteristics of the SCFETs are shown in Figure 3. The best results are obtained from devices of **1**, which shows the highest mobility of 3.6 cm^2 V^{-1} s^{-1} with an on/off ratio of 1.9×10^6 and a low threshold voltage of 6.7 V. Here, the mobilities (μ) were calculated in the saturation regime by the following equation: $I_D = \mu C_i(W/2L)(V_G - V_T)^2$, where I_D is the drain current, μ is the field-effect mobility, C_i is the gate dielectric capacitance, W and L are the channel width and length, respectively, and V_T is the threshold voltage. The highest mobilites of the SCFETs were 10, 80, and 130

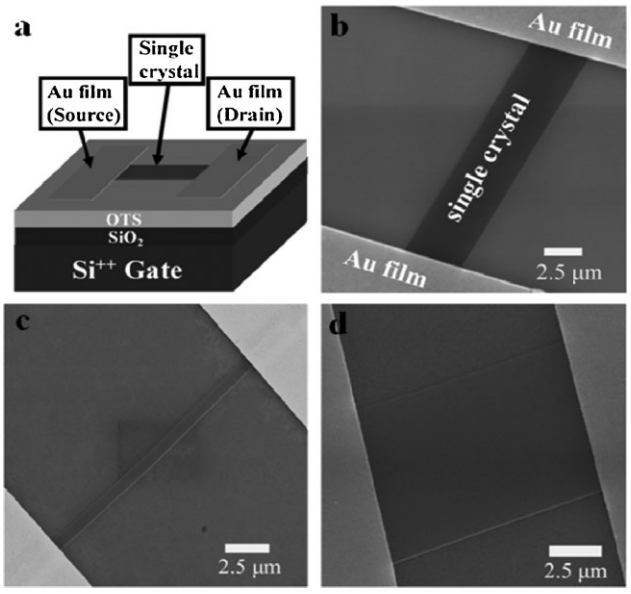

Figure 2. a) Schematic structure of a SCFET device based on an individual single-crystalline ribbon of PBBTZ. b–d) SEM images of typical SCFET devices based on individual single-crystalline ribbons of **1**, **2**, and **3**, respectively.

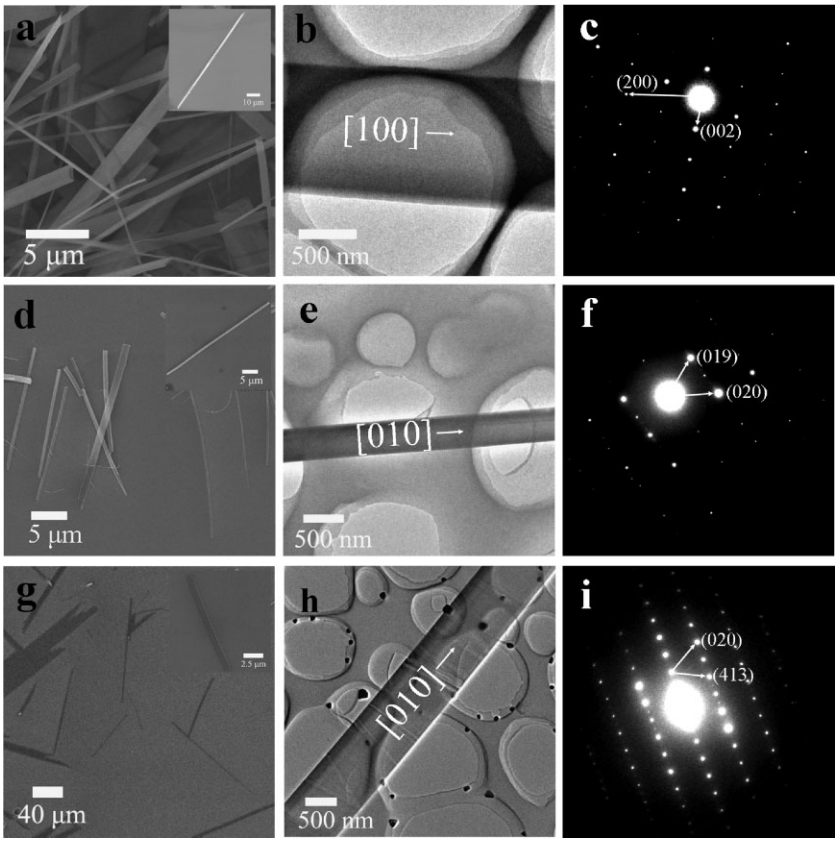

Figure 1. a,d,g) SEM images of large area single crystalline ribbons of **1**, **2**, and **3**, the insets show individual single-crystalline ribbons, respectively. b,e,h) TEM images of individual single-crystalline ribbons of **1**, **2**, and **3**, and c,f,i) their corresponding selected-area electron diffraction (SAED) patterns.

times higher than those of the thin film devices of **1**, **2**, and **3**, respectively.[23] Based on the individual single-crystalline ribbons of **1–3**, a total of 100 SCFET devices were fabricated and examined. Their performance data, including field-effect mobility (μ), on/off current ratio (I_{on}/I_{off}), and threshold voltage (V_T) are summarized in Table 1. It is noticed that the mobilities of the devices exhibit a relatively wide distribution, which might be due to the difference in the quality of the used crystals and the influence of device physics during their fabrication. It is well known that many factors, such as the position and deposition process of the source/drain electrodes, i.e., the precise orientation of the electrodes with respect to the π-stacking axis of the crystals, the gate electrode, the used material and flatness of the insulating layer, the quality of the crystal and crystal-insulator interface, etc. could affect the device performance, i.e., the value of the mobility. It was found that near 75% of the devices of compound **1** exhibited a mobility >0.1 cm^2 V^{-1} s^{-1} with the highest mobility of 3.6 cm^2 V^{-1} s^{-1} (Fig. S4), which indicates the prospective future of the compound in organic electronics.

One of the challenges for the industrial utilization of organic electronics is environmental stability. Besides high mobility, PBBTZ SCFETs also exhibit excellent stability. Figure S5 shows the stability of a typical PBBTZ **1** SCFET stored at room temperature in air.

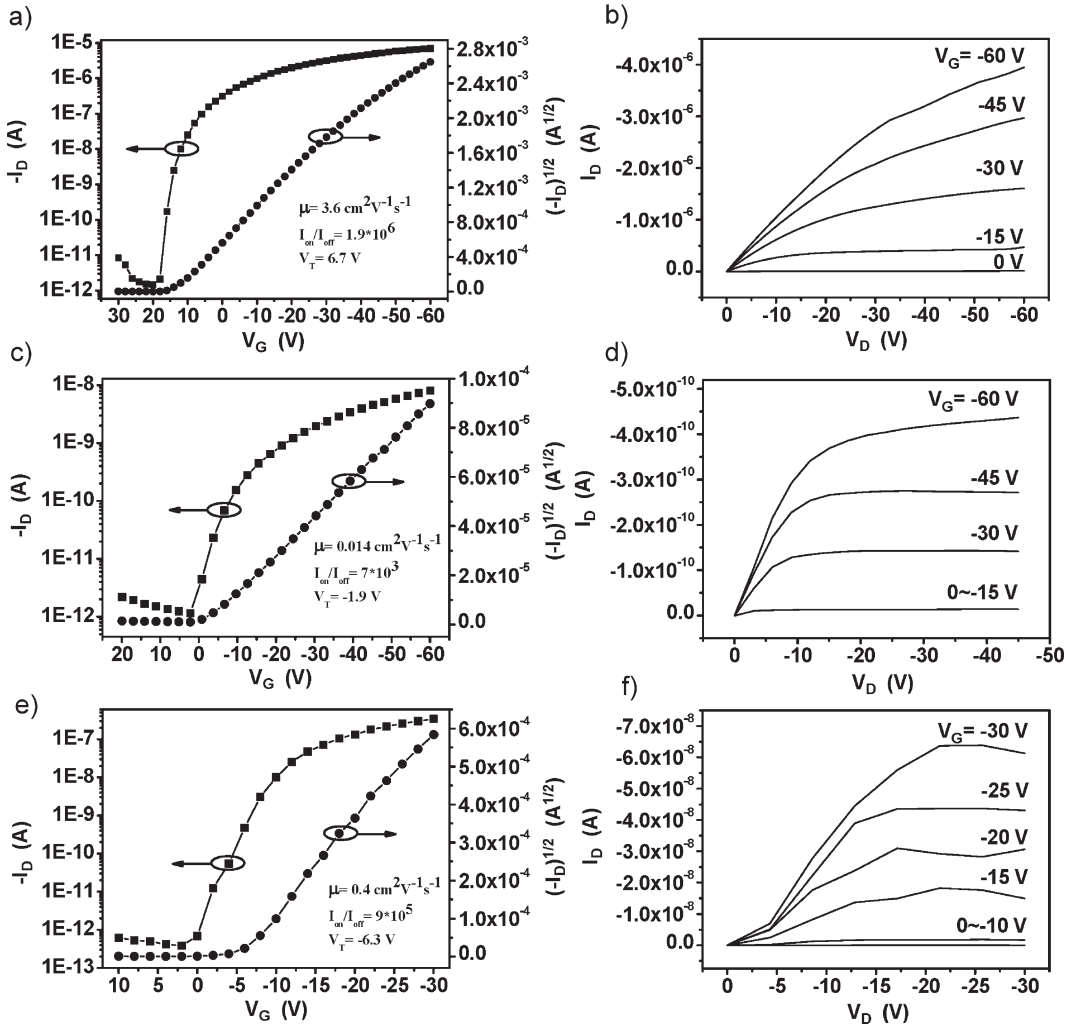

Figure 3. a) Typical transfer curve ($V_D = -60$ V) and b) the corresponding output curve of a SCFET based on an individual single-crystalline ribbon of **1**, with $W/L = 2.38$ μm/9.12 μm. c) Typical transfer curve ($V_D = -60$ V) and d) the corresponding output curve of a SCFET based on an individual single-crystalline ribbon of **2**, with $W/L = 0.89$ μm/19.13 μm. e) Typical transfer curve ($V_D = -30$ V) and f) the corresponding output curve of a SCFET based on an individual single-crystalline ribbon of **3**, with $W/L = 8.82$ μm/17.5 μm.

During a long period of one year, both the mobility and the on/off ratio of the device are maintained at high values without obvious decrease.

The substitution effects at the central pyrrole *N*-atom of PBBTZ were theoretically studied in order to investigate the relationship between crystal structure and charge carrier mobility. It is believed that a hopping mechanism dominates the charge transport process of organic semiconductors at room temperature. The charge transfer process can be considered as a self-exchange reaction, in which the reorganization energy and the electronic coupling parameters determine self-exchange reaction rates and, thus, the mobility.[26,27] The quantum chemical calculated reorganization energy of **1** (195 meV) and **3** (200 meV) are almost identical and about 15% lower than that of **2** (231 meV). It can be seen that the substitutions on the central pyrrole unit induces limited changes in the reorganization energy and the influence on the charge transport properties could be ignored, as the alkyl chain and phenyl group made no contribution to the frontier orbits of the whole molecules and have no effect on the charge delocalization of the cation of PBBTZs.

Table 1. FET performances of the PBBTZ **1–3** single-crystal devices.

PBBTZ	μ [$cm^2V^{-1}s^{-1}$]	I_{on}/I_{off}	V_T [V]	No. of devices
1	0.01 to 3.6	10^4 to 8×10^6	−9 to + 13	40
2	10^{-4} to 0.014	6×10^2 to 10^4	−18 to + 4	30
3	3×10^{-4} to 0.4	2×10^3 to 9×10^5	−18 to −0.3	30

The transfer integral (V_h) for all the hopping pathways of PBBTZ **1–3** are listed in Table S2 of the Supporting Information. According to a neighbor transfer integral analysis, we found that crystals of alkyl- and phenyl-group substituted PBBTZ molecules (**2** and **3**) display a one-dimensional transport character along the π-stacking direction, while other directions were relatively

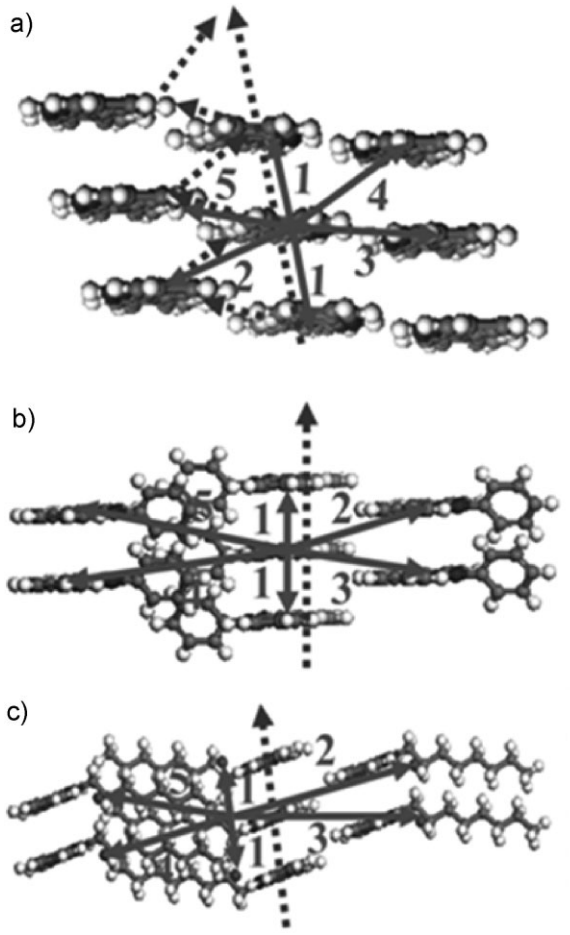

Figure 4. Transfer integral analysis of the crystals of a) **1**, b) **2**, and c) **3**. (The solid line represents neighbor molecules as charge transfer pathways, the dashed lines label the possible charge transfer route.)

difficult for transport (Fig. 4b,c). As discussed above, crystal structures of **2** and **3** show stacking along the [010] direction. The intermolecular distance in the other direction is so large that electronic coupling is very weak and can be neglected (as the transfer integral values of the pathways 2–5 shown in Table S2 are relatively low). There is a different intermolecular displacement along the molecular long axis between **2** and **3**. As mentioned in the section on crystal structures (see Supporting Information), it is important to note that the intermolecular relative slide distance for **3** is larger than that of **2**, but the molecular wavefunction overlap is larger for **3** than that of **2**, and intermolecular anti-bonding interactions are formed for **3**. PBBTZ **3** has a much larger electronic coupling than that of **2**. This means that the intermolecular displacement is critical for the determination of the intermolecular π–π interactions. Therefore, the intermolecular stacking style for **3** will be favorable for π–π intermolecular charge transport. From the calculated charge transfer parameters, we can infer that single crystal devices of **3** will have a higher mobility than devices of **2**. Such a result is fully consistent with the experimental data in Table 1.

However, crystal **1** in particular displayed two-dimensional transport properties (Fig. 4a). We found that there is large electronic coupling because of the interstacking S…S contacts and hydrogen bonds. The transfer integral along the stacking direction ($V_1 = -33.054$ meV) is much smaller than that of **3**, but two-dimensional electronic couplings were observed with $V_2 = 85.624$ meV, $V_3 = 3.451$ meV, $V_4 = 2.318$ meV, and $V_5 = -18.121$ meV (Table S2). The single crystal of **1** displayed the highest charge transport mobility among the three crystals (Table 1). It seems that the Marcus theory does not apply here. In fact, different defects may exist in the crystal, which will act as charge-carrier traps and lower the electrical transport properties of the crystal. Previously, Bao et al. reported that rubrene crystals showed poorer conformability and poorer interfacial contacts to the dielectric interface when the size of the crystals increased.[28] We also found that the smaller the crystal, the higher the mobility observed in SCFETs based on crystalline ribbons of a cyclic triphenylamine dimer.[29] This is also a result of the increase in quality when the crystal size is reduced. In a one-dimensional crystal the electrical transport should be more easily interrupted by the defects, whereas in a two-dimensional crystal the influence of the defects along the π–π stacking direction will be compensated by the electrical transport along other directions. So, the crystal with two-dimensional electrical transport capability should possess a higher tolerance towards the defects. This could be the possible reason why crystals of **1** display a higher mobility than those of **3**.

In summary, crystal structures, SCFETs, and quantum chemical calculations of PBBTZs **1–3** have been studied. The results indicate that the different substitutes on the *N*-atom of the central pyrrole units result in different crystal structures and different charge transport properties. When comparing the device made from **1** with the devices based on the other two crystals, it displays the highest mobility of 3.6 $cm^2\ V^{-1}s^{-1}$ in SCFETs. Besides the good performance, excellent environmental stability was also observed on the SCFETs of **1**. During a testing period of one year, no significant decrease in the performance could be detected. The above results indicate that the PBBTZs are promising organic semiconductors, and further improvement of the transport properties may be achieved by chemical tailoring.

Experimental

Growth of the Single Crystals and Device Fabrication: PBBTZ **1–3** were synthesized as previously described [23] and purified by gradient sublimation twice before use as the source materials for the growth of single crystals. PBBTZ **1–3** single crystalline ribbons were grown by physical vapor transport processes in a horizontal tube furnace as reported [24]. A quartz boat with powders of **1–3** were placed at the high-temperature zone and vaporized at 165, 145, and 110 °C, respectively. High-purity Ar was used as the carrier gas at a rate of 150 $mL{\cdot}min^{-1}$, and the system was evacuated by a mechanical pump. Single-crystalline sub-micrometer ribbons of **1–3** were obtained in the low-temperature zone on octadecyltrichlorosilane (OTS)-treated Si/SiO_2 substrates. The deposition time was 3 h. The Si/SiO_2 substrate was a heavily doped *n*-type Si wafer with a 500 nm thick SiO_2 layer and a capacitance of 7.5 $nF{\cdot}cm^{-2}$. The device fabrication process was carried out with a Micromanipulator 6150 probe station as reported [10,25]. Thin Au films (~100 nm thick) were glued onto the individual single crystalline sub-micrometer ribbons by van der Waals forces with the help of the mechanical probes and functioned as source/drain electrodes. The n-type Si substrate functioned as the gate electrode.

Measurements: SEM images were obtained with a Hitachi S-4300 s.e. (Japan). TEM and SAED measurements were carried out on a JEOL 2010

(Japan). The FET measurements were carried out with a Micromanipulator 6150 probe station in a clean and metallically shielded box at room temperature in air, and recorded using a Keithley 4200 SCS.

Quantum Chemical Calculation: The reorganization energies are calculated at the DFT/6-31G* level with the hybrid B3 LYP function, as implemented in the Gaussian 03 package [30]. The normal-mode analysis and the Huang–Rhys factors, as well as the reorganization energies of normal modes for both neutral and charged molecules, are obtained through the DUSHIN program developed by Reimers [31]. The electronic coupling term V is calculated through Equation 1 [6,32]:

$$V = \frac{H_{12} - \frac{1}{2}(H_{11} + H_{22})S_{12}}{1 - S_{12}^2} \quad (1)$$

The H matrix elements are calculated by $H_{ij} = \langle \phi_i | H | \phi_j \rangle$, where ϕ_i and ϕ_j represent the highest occupied molecular orbitals (HOMOs) for hole transport of isolated molecules in the dimer. H is the self-consistent Hamiltonian matrix of the dimer and S_{12} is the overlap integral. The electronic coupling is calculated at the DFT/6-31G* level with the pw91pw91 function, as implemented in the Gaussian 03 package [30].

Acknowledgements

The authors acknowledge the financial support from National Natural Science Foundation of China (20721061, 50725311, 20952001), Ministry of Science and Technology of China, and the Chinese Academy of Sciences. Supporting Information is available online from Wiley InterScience or from the author.

Received: January 10, 2010
Revised: February 3, 2010
Published online: April 7, 2010

[1] A. R. Murphy, J. M. J. Fréchet, *Chem. Rev.* **2007**, *107*, 1066.
[2] J. Zaumseil, H. Sirringhaus, *Chem. Rev.* **2007**, *107*, 1296.
[3] S. Allard, M. Forster, B. Souharce, H. Thiem, U. Scherf, *Angew. Chem. Int. Ed.* **2008**, *47*, 4070.
[4] M. Mas-Torrent, C. Rovira, *Chem. Soc. Rev.* **2008**, *37*, 827.
[5] Y. D. Park, J. A. Lim, H. S. Lee, K. Cho, *Mater. Today* **2007**, *10*, 46.
[6] V. Coropceanu, J. Cornil, D. A. da Silva Filho, Y. Olivier, R. Silbey, J.-L. Brédas, *Chem. Rev.* **2007**, *107*, 926.
[7] R. W. I. de Boer, M. E. Gershenson, A. F. Morpurgo, V. Podzorov, *Phys. Stat. Sol. A* **2004**, *201*, 1302.
[8] C. Reese, Z. Bao, *J. Mater. Chem.* **2006**, *16*, 329.
[9] C. Reese, Z. Bao, *Mater. Today* **2007**, *10*, 20.
[10] Q. Tang, L. Jiang, Y. Tong, H. Li, Y. Liu, Z. Wang, W. Hu, Y. Liu, D. Zhu, *Adv. Mater.* **2008**, *20*, 2947.
[11] A. L. Briseno, S. C. B. Mannsfeld, S. A. Jenekhe, Z. Bao, Y. Xia, *Mater. Today* **2008**, *11*, 38.
[12] E. Menard, V. Podzorov, S.-H. Hur, A. Gaur, M. E. Gershenson, J. A. Rogers, *Adv. Mater.* **2004**, *16*, 2097.
[13] V. C. Sundar, J. Zaumseil, V. Podzorov, E. Menard, R. L. Willett, T. Someya, M. E. Gershenson, J. A. Rogers, *Science* **2004**, *303*, 1644.
[14] V. Podzorov, E. Menard, A. Borissov, V. Kiryukhin, J. A. Rogers, M. E. Gershenson, *Phys. Rev. Lett.* **2004**, *93*, 086602.
[15] L. B. Roberson, J. Kowalik, L. M. Tolbert, C. Kloc, R. Zeis, X. Chi, R. Fleming, C. Wilkins, *J. Am. Chem. Soc.* **2005**, *127*, 3069.
[16] C. Reese, W.-J. Chung, M. M. Ling, M. Roberts, Z. Bao, *Appl. Phys. Lett.* **2006**, *89*, 202108.
[17] Q. Tang, H. Li, M. He, W. Hu, C. Liu, K. Chen, C. Wang, Y. Liu, D. Zhu, *Adv. Mater.* **2006**, *18*, 65.
[18] Q. Tang, H. Li, Y. Liu, W. Hu, *J. Am. Chem. Soc.* **2006**, *128*, 14634.
[19] Y. Zhou, W. Liu, Y. Ma, H. Wang, L. Qi, Y. Cao, J. Wang, J. Pei, *J. Am. Chem. Soc.* **2007**, *129*, 12386.
[20] A. L. Briseno, S. C. B. Mannsfeld, X. Lu, Y. Xiong, S. A. Jenekhe, Z. Bao, Y. Xia, *Nano Lett.* **2007**, *7*, 668.
[21] A. L. Briseno, S. C. B. Mannsfeld, C. Reese, J. M. Hancock, Y. Xiong, S. A. Jenekhe, Z. Bao, Y. Xia, *Nano Lett.* **2007**, *7*, 2847.
[22] L. Jiang, J. Gao, E. Wang, H. Li, Z. Wang, W. Hu, L. Jiang, *Adv. Mater.* **2008**, *20*, 2735.
[23] W. Hong, Z. Wei, H. Xi, W. Xu, W. Hu, Q. Wang, D. Zhu, *J. Mater. Chem.* **2008**, *18*, 4814.
[24] R. A. Laudize, C. Kloc, P. G. Simpkins, T. Siegrist, *J. Cryst. Growth* **1998**, *187*, 449.
[25] Q. Tang, Y. Tong, H. Li, Z. Ji, L. Li, W. Hu, Y. Liu, D. Zhu, *Adv. Mater.* **2008**, *20*, 1511.
[26] G. Nan, X. Yang, L. Wang, Z. Shuai, Y. Zhao, *Phys. Rev. B* **2009**, *79*, 115203.
[27] L. Tan, L. Zhang, X. Jiang, X. Yang, L. Wang, Z. Wang, L. Li, W. Hu, Z. Shuai, L. Li, D. Zhu, *Adv. Funct. Mater.* **2009**, *19*, 272.
[28] A. L. Briseno, R. J. Tseng, M. M. Ling, E. H. L. Talcao, Y. Yang, F. Wudl, Z. Bao, *Adv. Mater.* **2006**, *18*, 2320.
[29] R. Li, H. Li, Y. Song, Q. Tang, Y. Liu, W. Xu, W. Hu, D. Zhu, *Adv. Mater.* **2009**, *21*, 1605.
[30] M. J. Frisch, G. W. Trucks, H. B. Schlegel, G. E. Scuseria, M. A. Robb, J. R. Cheeseman, J. A. Montgomery, Jr, T. Vreven, K. N. Kudin, J. C. Burant, J. M. Millam, S. S. Iyengar, J. Tomasi, V. Barone, B. Mennucci, M. Cossi, G. Scalmani, N. Rega, G. A. Petersson, H. Nakatsuji, M. Hada, M. Ehara, K. Toyota, R. Fukuda, J. Hasegawa, M. Ishida, T. Nakajima, Y. Honda, O. Kitao, H. Nakai, M. Klene, X. Li, J. E. Knox, H. P. Hratchian, J. B. Cross, C. Adamo, J. Jaramillo, R. Gomperts, R. E. Stratmann, O. Yazyev, A. J. Austin, R. Cammi, C. Pomelli, J. W. Ochterski, P. Y. Ayala, K. Morokuma, G. A. Voth, P. Salvador, J. J. Dannenberg, V. G. Zakrzewski, S. Dapprich, A. D. Daniels, M. C. Strain, O. Farkas, D. K. Malick, A. D. Rabuck, K. Raghavachari, J. B. Foresman, J. V. Ortiz, Q. Cui, A. G. Baboul, S. Clifford, J. Cioslowski, B. B. Stefanov, G. Liu, A. Liashenko, P. Piskorz, I. Komaromi, R. L. Martin, D. J. Fox, T. Keith, M. A. Al-Laham, C. Y. Peng, A. Nanayakkara, M. Challacombe, P. M. W. Gill, B. Johnson, W. Chen, M. W. Wong, C. Gonzalez, J. A. Pople, *Gaussian 03, Revision A.1*, Gaussian, Inc, Pittsburgh PA **2003**.
[31] J. R. Reimers, *J. Chem. Phys.* **2001**, *115*, 9103.
[32] E. F. Valeev, V. Coropceanu, D. A. da Silva Filho, S. Salman, J.-L. Brédas, *J. Am. Chem. Soc.* **2006**, *128*, 9882.